Adamantane Substitution Effects on Crystallization and Electrooptical Properties of Epindolidione and Quinacridone Dyes

Jan Richtar[+],[a] Martin Ciganek[+],[a] Anna Jancik Prochazkova,[a] Alexander Kovalenko,[a] Hathaichanok Seelajaroen,[b] Matouš Kratochvíl,[a] Martin Weiter,[a] Cigdem Yumusak,[a, b] Niyazi Serdar Sariciftci,[b] Vladimir Lukeš,[c] and Jozef Krajcovic*[a]

The synthesis, experimental and theoretical study of the novel air-stable four adamantane-bearing dyes based on the *trans*-epindolidione (**EPI**) and *trans*-quinacridone (**QA**) cores are presented. Compared to the parent **EPI** and **QA**, the methyl-/ethyladamantyl substitution ensures that their structural stability in crystals is preserved due to the self-organizing properties of adamantyl groups. The investigated materials are solution-processable in common organic solvents and possess excellent thermal stability. The very good solubility was achieved by a one-step short and easy synthesis, which resulted in moderate yields of a new family of synthesized dyes. The ethyladamantyl **EPI** derivative (**3**) exhibits a unique rise in thermal stability reaching 412 °C. The resulting electrochemical band gap carried out on thin-film evaporated on ITO-coated glass electrodes was in the range of 2.4–2.5 eV. The experimental HOMO energies range from −6.2 to −6.0 eV, and LUMO energies lay between −3.7 and −3.5 eV. The prepared compounds are characterized by strong fluorescence in solutions and in powder, suggesting a decrease in the extent of non-radiative relaxation processes.

1. Introduction

Organic high-performance pigments (HPPs) have fascinated scientists in recent years because of their unique properties and potential applications in various fields of organic electronics.[1–7] Substantial attention has been given to their combination of promising electrical and optical properties, as well as their processability and stability. The semiconducting properties of HPPs have been well known since the 1990s, and their fine molecular tuning allows for changing their optical, electrical, electrochemical or thermal properties or solubility and processability.[8,9]

Among HPP, epindolidione (**EPI**) and quinacridone (**QA**) have been extensively investigated due to their high thermal and chemical/photochemical stability, non-toxicity and strong two-dimensional molecular associations in the crystal structure via hydrogen bonding, and they have been employed in a variety of applications. Moreover, these pigments are unique synthetic building blocks with a tunable molecular framework for the preparation of structurally advanced organic semiconductors.[10–18]

Głowacki et al.[19] described how the effects of *H*-bonding and chirality might compete and significantly affect the formation of the resulting quinacridone structures upon deposition on the Ag(111) surface. Very recently, materials for non-linear optics where quinacridone acts as an electron acceptor have been studied.[20] More recently, a study describing the proper deposition techniques for the preparation of quinacridone thin films in the context of organic electronic devices has been published.[21] Furthermore, Koehler et al.[22] reported two sets of model system **EPI** and **QA** equipped with the lock-and-key system of biotin and avidin via topography and recognition (TREC)-atomic force microscopy (AFM) for biological applications.

However, materials based on soluble, *N*,*N*′-alkylated quinacridones have also found a range of applications in organic electronics. Shaheen et al.[23] described the charge transfer efficiency enhancement in organic-light emitting diodes based on soluble quinacridone-doped tris(8-hydroxyquinoline) aluminium (Alq_3) devices. The OLED emission layers based on soluble dialkylquinacridones as co-dopants have also been published to describe the interactions between the corresponding molecules and the metallic substrate.[24] Moreover, Nguyen

[a] *Dr. J. Richtar,[+] Dr. M. Ciganek,[+] Dr. A. J. Prochazkova, Dr. A. Kovalenko, Dr. M. Kratochvíl, Prof. M. Weiter, Dr. C. Yumusak, Prof. J. Krajcovic*
Brno University of Technology,
Faculty of Chemistry
Materials Research Centre
Purkyňova 118, 612 00 Brno (Czech Republic)
E-mail: krajcovic@fch.vut.cz
[b] *Dr. H. Seelajaroen, Dr. C. Yumusak, Prof. N. S. Sariciftci*
Linz Institute for Organic Solar Cells (LIOS),
Physical Chemistry
Johannes Kepler University Linz
Altenbergerstraße 69, 4040 Linz (Austria)
[c] *Prof. V. Lukeš*
Institute of Physical Chemistry and Chemical Physics
Faculty of Chemical and Food Technology
Slovak University of Technology in Bratislava
Radlinského 9, SK-812 37 Bratislava
(Slovakia)
[+] *These authors contributed equally to this work.*

Supporting information for this article is available on the WWW under https://doi.org/10.1002/cptc.202100127

et al.[25] have described the effective utilization of quinacridone salts as electron injection layers in polymer light-emitting diodes (PLEDs). *N,N′*-dimethylquinacridone has also been described as a key donor material in an active bulk-heterojunction layer of an organic photodiode device (OPD) for frequency response enhancement. This study provides a valuable overview of the parameters for efficient organic color-sensitive OPDs aiming at an artificial retina.[26] Additionally, alkylated quinacridones exhibit increased intracellular permeability compared to unsubstituted QA. Shangguan et al.[27] discovered a specific binding ability of selected alkylated quinacridone derivatives (e.g. *N,N′*-bis(5-bromopentyl)-quinacridone) to the G-quadruplexes of DNA. The studied derivatives preserved low cytotoxicities, suggesting their potential to act as molecular probes for live-cell imaging.

Besides the excellent properties of *N,N′*-non-alkylated (*NH*-free) **EPI** and **QA**, new structural alternatives in which no *H*-bonding occurs were intensively investigated. These comprise mainly alkylated derivatives with linear or branched alkyl substituents incorporated to increase the solubility and thus the processability of the pigments.[28–31] However, such substitution disrupts the intermolecular hydrogen bonds, leading to changes in the molecular organization in the solid-state and other physicochemical properties, particularly optical and electrical properties, thermal and oxidative stability. In many cases, *N*-alkyl substitutions of pigments also significantly reduce the melting points and thermal degradation of the resulting materials detectable by DSC and TGA methods.[32] The effect of *N*-alkylation of **EPI** and **QA** on the optical properties is most evident in the electroluminescent applications. Even though the absorption and emission spectra are not significantly influenced, the tendency of the pigments to aggregate due to π-π interactions results in emission quenching.[33,34] An efficient approach improving the fluorescence quantum yields (Φ_F) is represented by the introduction of bulky substituents at the nitrogen atoms that suppressed the π-π interactions.[35]

Breaking the hydrogen bonds by *N*-alkylation may lead to poor structural organization, worsening the charge transport characteristics.[36] On the other hand, the careful choice of alkyl substituent and processing conditions may provide a highly ordered crystalline organization of the material with the efficient interconnection of crystalline domains and intermolecular π-orbital overlap, thus providing charge carrier mobilities even higher than that of the parent material.[37] An effective strategy to balance the benefits and drawbacks of the *N*-alkyl substitution lies in the introduction of the bulky alkyl substituents connected with adamantane moiety. The incorporation of sterically demanding but highly symmetrical adamantane moiety is known to induce highly-ordered molecular organization in the solid state due to effective van der Waals interactions. These interactions lead to self-organization between adamantane moieties, thus overcoming the lack of hydrogen bonding and providing the material with high thermal stability. At the same time, the solubility and processability of these systems remain preserved.[38,39]

In the present work, we report the synthesis, experimental and theoretical study of the novel four adamantane-bearing dyes based on the linear *trans*-**QA** and *trans*-**EPI** cores (Figures 1 and 2). The partial aims of this study are: (1) to present the effective synthetical route of the studied molecules; (2) to characterize the chemical structural and electronic properties; (3) to deduce the π-stacking ability of the studied molecules from the experimental X-ray structures; (4) to calculate the lowest energies of optical transitions for the gas-phase and solvent environment; and (5) to theoretically estimate drift mobilities for dimers in crystals at room temperature ($T = 298.15$ K). Finally, the obtained experimental and theoretical results will be compared with the experimental data available for **EPI** and **QA**.

2. Results and Discussion

The alkylated dyes were prepared by the nucleophilic substitution of the NH-free quinacridone and epindolidione by ethyladamantyl bromide or methyladamantyl bromide, respectively (Figure 2). The alkylation provided the target compounds in low to moderate yields. We hypothesize that the observed low selectivity and moderate yields result from the steric factors given the bulkiness of the adamantyl moiety. Generally, higher yields were obtained for the ethyladamantyl dyes **1** and **3**; in both the bulky adamantyl moiety is more distant from the electrophilic center at the alkylating reagent than for the dyes **2** and **4**. Moreover, low selectivity can also be reasoned by the presence of the pair of competing *O* and *N* nucleophilic centers at the deprotonated dyes, providing a possibility for the formation of various undesired side-products.

2.1. Thermal stability characterization

The thermal properties of the alkylated dyes **1** to **4** were investigated by thermogravimetric analyses. Both reference quinacridone (**QA**) and epindolidione (**EPI**) are known to be highly thermally stable H-bonded dyes with decomposition temperatures of 535 °C and 400 °C,[14] respectively (Table 1), given the strong intermolecular hydrogen bonding. The TGA measurements of the dyes **1** to **4** pointed out their excellent thermal stability. Both quinacridone derivatives **1** and **2** showed a diminished decomposition temperature, but one still exceeding 400 °C, not often observed for the small organic molecules. On the other hand, epindolidione derivate **4** showed a decomposition temperature comparable to NH-free dye, while compound **3** decomposed even at a higher temperature

Table 1. TGA analyses data.

Compound	Temperature of decomposition/[°C]
QA	535[14]
1	463
2	443
EPI	400[14]
3	412
4	397

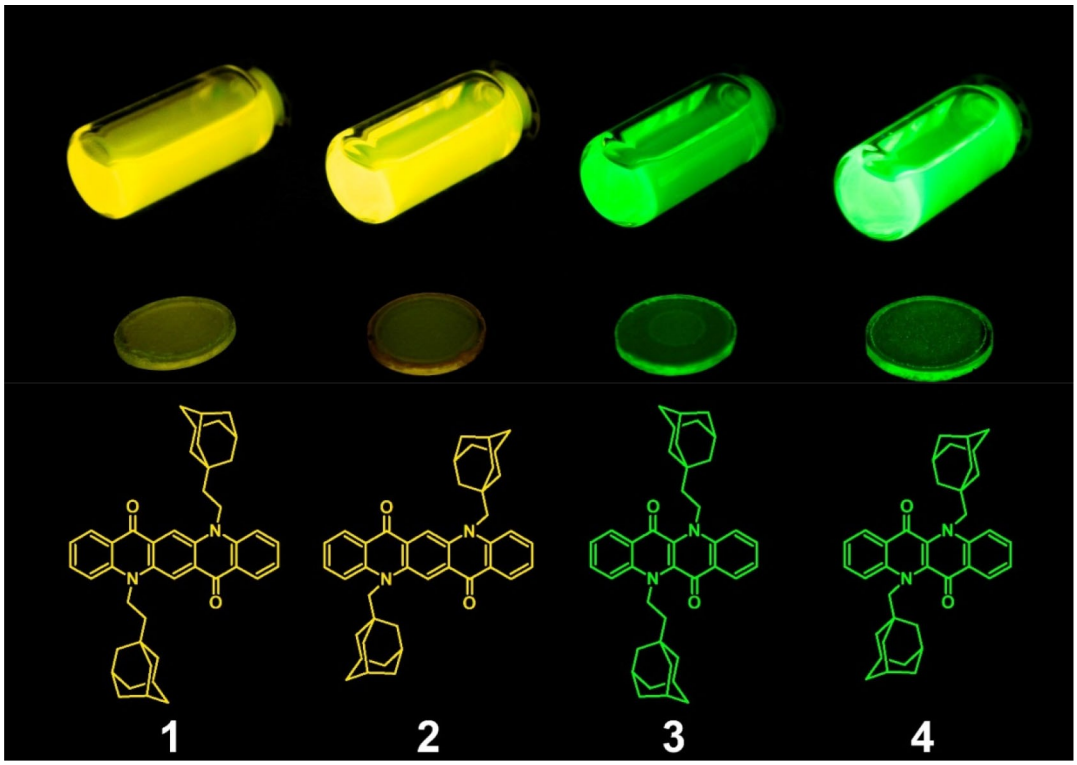

Figure 1. Molecular structures and photographs of the studied adamantyl-substituted derivatives of quinacridone (**1**, **2**) and epindolidione derivatives (**3**, **4**) under irradiation with UV light (365 nm) in chloroform with a concentration of 10^{-3} M (top) and solid-phase (bottom).

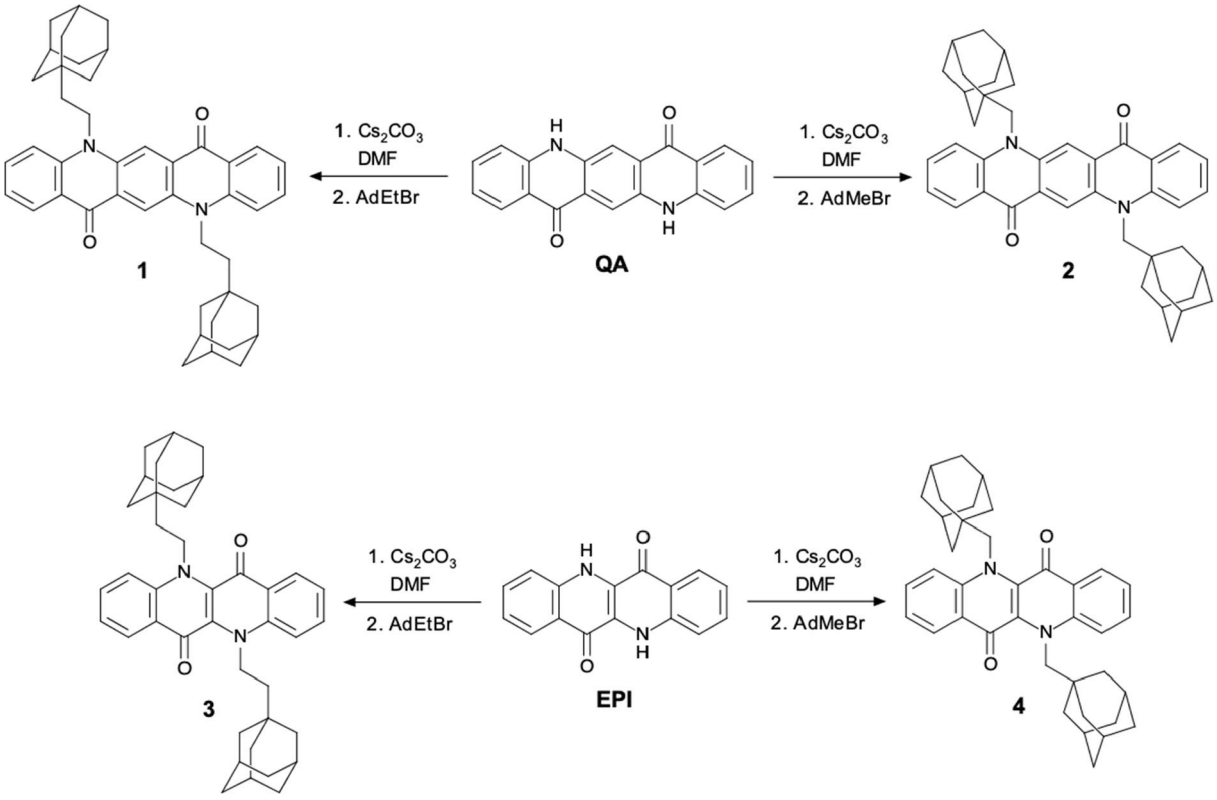

Figure 2. Synthesis of adamantyl-moiety bearing dyes.

compared to NH-free epindolidione (Table 1, thermogravimetric records are shown in the Supporting information as Figure S1). The alkylation of such kind suppresses the hydrogen bonding, which often results in lowering the thermal stability. On the other hand, we hypothesize that introducing the adamantyl-containing substituents provides the molecules with strong molecular packing ability due to the self-organizing effect of the highly symmetrical and rigid adamantane moiety via van der Waals interactions, thus having a positive effect on the thermal stability of the target molecules.

2.2. Molecular geometry and crystal structure

The optimal gas-phase geometries of **QA** and **EPI** molecules are planar, and they belong to the C_{2h} point group. The addition of side adamantyl groups to parent cores changes the symmetry point group to Ci. As it is illustrated in Figure S2, the steric repulsion between (C)═O and (N)–CH_2– atoms of added groups leads to the planarity perturbation of central rings in **3** and **4** molecules. The π-stacking ability of aromatic rings may represent the key factor that primarily affects the thermal stability and macroscopic electrical properties of the solid-state sample. Moreover, the incorporated adamantyl moieties affect solid-state organization via adamantyl-induced packing and consequently strongly contribute to the thermal stability or significant fluorescence. For the reference molecules, the presence of –NH and C═O groups can support the formation of quadruple weak hydrogen bonds. The theoretical calculations of the ideal model planar arrangement of **QA** and **EPI** molecules indicate that the intermolecular hydrogen bond distances are 1.91 and 1.94 Å (Figure S3 and S4), respectively. The corresponding interaction energies are (−91.7 kJ mol^{-1} for **QA** and −75.3 kJ mol^{-1} for **EPI**. The molecular packing of EPI in X-ray structure (Figure S5) features π-π stacking as well and hydrogen bonds between (N)–H···O═(C) atoms. Moieties in the crystal structure form parallel-shifted stacks with a π-π distance of 3.94 Å, which is longer than the interplanar distance in a graphene sheets stack (3.35 Å).[40] The estimated BSSE-free interaction dimer energy is −56.6 kJ mol^{-1}. According to the theoretical calculations of ideal planar dimers mentioned above, the second selected dimer is planar, which is slightly shifted along the longest axial axis. The intermolecular hydrogen bond distances are shorter than 1.71 Å, and the interaction energy is −70.0 kJ mol^{-1}. The X-ray structures available in the literature on **QA** can possess triclinic or monoclinic space groups. Interestingly, the planar dimers are not present. As it is depicted in Figure 3, the parallel-shifted stacking dimers represent the most stable structures. The centroid-to-centroid distances are between 3.80 and 3.98 Å. The interaction energy for these dimers is higher by about 13 kJ mol^{-1} than for the corresponding **EPI** dimer. The presence of bulky adamantyl moieties blocks the formation of planar dimers fixed by hydrogen bonds, and the centroid-to-centroid distances are increased. The triclinic space group was identified for **1**, **2** and **4** molecules. The **EPI** core substituted by ethyladamantyl groups (**3**) crystallizes in the orthorhombic space group, and for this crystal structure, five different dimers were selected. The most stable parallel-shifted dimers have the largest **1** and **2** molecules. Due to the plane-to-plane stacking of conjugated cores, the interaction energies are −104.3 kJ mol^{-1} for **1** and −110.7 kJ mol^{-1} for **2**. Probably due to the planarity perturbation of central cores in smaller molecules **3** and **4**, the interaction energies of parallel-shifted dimers are smaller by around 50 kJ mol^{-1}. For the rest of the selected dimers, the adamantyl-induced packing determines the subsystem arrangement, and the corresponding interaction energies are lower than −40.0 kJ mol^{-1}.

2.3. Electrochemical properties

The energy levels of Highest Occupied (HOMO) and Lowest Unoccupied (LUMO) Molecular Orbitals are key parameters for assessing the p-type and n-type carrier injection ability and stability of the material, respectively. To determine HOMO and LUMO energy levels electrochemically, cyclic voltammetry was carried out on a thin-film of adamantyl-substituted quinacridones, and epindolidiones evaporated on ITO-coated glass as working electrodes. All compounds showed redox behaviors of their **QA** and **EPI** core structures .[13,41] The experimental energy levels of frontier molecular orbitals were obtained from the onset oxidation and onset reduction potentials (Table 2). The HOMO energy levels were in the range of −6.0 to −6.2 eV, while LUMO energy levels lay at between −3.5 and −3.7 eV. The resulting electrochemical band gap (E_{gap}) values were 2.4 to 2.5 eV, which were in the same range as **QA** and **EPI**.[13,41] These values are in reasonable ranges and suitable for the construction of molecular devices.

The B3LYP energies of frontier molecular orbitals for the gas-phase geometries differ from these experimental values. The HOMO energies are changed from −5.13 eV for **1** to −5.47 eV for **EPI**. The LUMO energies are between −2.02 eV for **3** to −2.17 eV for **QA**. For all investigated molecules, the HOMOs and LUMOs are delocalized only over the central part. As it is illustrated in Figure 4 for molecules **1** and **3**, the lobes of HOMOs are uniformly delocalized over the longest axial direction and bonds in the vicinity of heteroatoms. On the other hand, the lobes of LUMO are mostly delocalized over the bonds parallel with the smaller axial direction. The small electron clouds are also indicated on the substituent atoms directly connected to the central cores.

Table 2. The experimental values of the energies of frontier molecular orbitals for the thin films. The B3LYP values of FMO energies (in parentheses) and internal reorganization energies (λ) calculated for the gas-phase. All values are in eV.

	HOMO	LUMO	λ^+	λ^-
QA	(−5.32)	(−2.17)	0.141	0.234
EPI	(−5.47)	(−2.08)	0.163	0.269
1	−6.2 (−5.13)	−3.7 (−2.06)	0.141	0.238
2	−6.0 (−5.14)	−3.5 (−2.04)	0.156	0.241
3	−6.1 (−5.26)	−3.7 (−2.02)	0.208	0.363
4	−6.2 (−5.25)	−3.7 (−2.03)	0.187	0.388

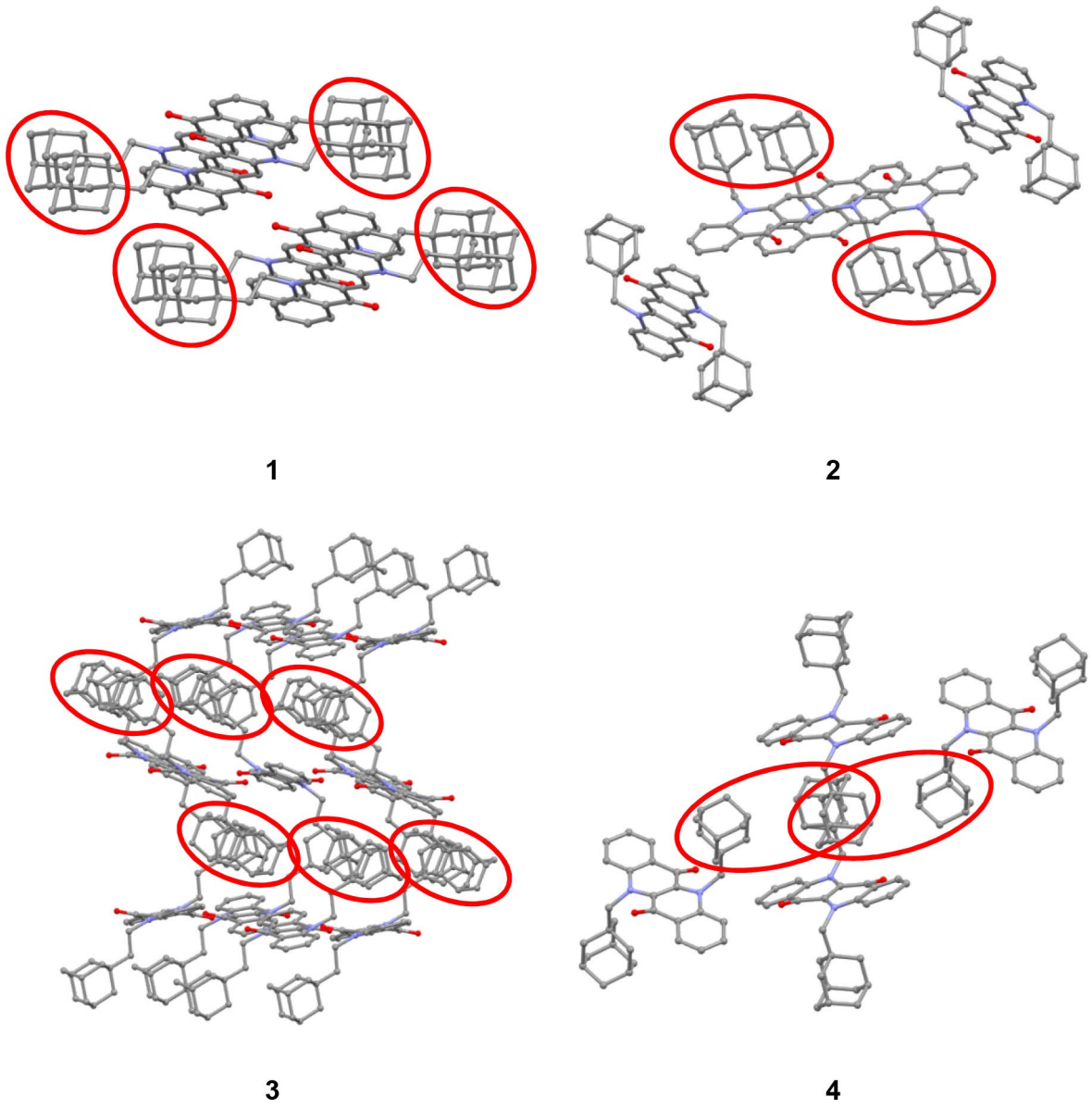

Figure 3. Adamantyl-induced packing of methyl- and ethyladamantyl-substituted derivatives deduced from X-ray structures. Hydrogen atoms are hidden. The colored bubbles indicate the strong dimer interactions between adamantyl moieties.

The reorganization energy $\lambda^{\pm}$ is the dominant quantity reflecting the geometrical changes upon electric charging. The calculated values for both charged states are listed in Table 2. The B3LYP hole reorganization energies of the **EPI** and **QA** molecules connected with the formation of the cationic state (λ^{+}) are 0.141 and 0.163 eV, respectively. For example, the theoretical value for pentacene, as reference p-semiconductor, is 0.100 eV .[42] The electron reorganization energies (λ^{-}) are two times higher, i.e. 0.234 eV for **QA** to 0.388 eV for **4**. The estimated value for the fluorinated pentacene, as the representative n-semiconductor, is 0.246 eV.

Considering the hopping mechanism and Marcus theory, drift mobilities of electron transfer were not found for the dimers of reference **QA** and **EPI** molecules (see Figure S5). On the other hand, the planar and parallel-shifted dimers of the smaller **EPI** molecule have hole drift mobilities of 0.56 and 0.33 $cm^2V^{-1}s^{-1}$. In the case of **QA**, only parallel-shifted dimers identified in both crystal modifications exhibit comparable mobility values, i.e. 0.55 $cm^2V^{-1}s^{-1}$ for the triclinic space group and 0.27 $cm^2V^{-1}s^{-1}$ for the monoclinic space group. The experimental hole mobility measured by Głowacki et al.[2] for the sublimated quinacridone is around 0.2 $cm^2V^{-1}s^{-1}$. The EPI material demonstrated mobility in the range of 0.9 to 1.5 $cm^2V^{-1}s^{-1}$. These higher macroscopic mobility values probably represent the statistical average of all possible dimers contributing to the charge transfer processes. Although the addition of the adamantyl groups decreases theoretical hole drift mobilities for epindolidione derivatives, improved hole mobilities between dimers based on larger **3** and **4** molecules are predicted (see Figure S6). Interestingly, the non-negligible

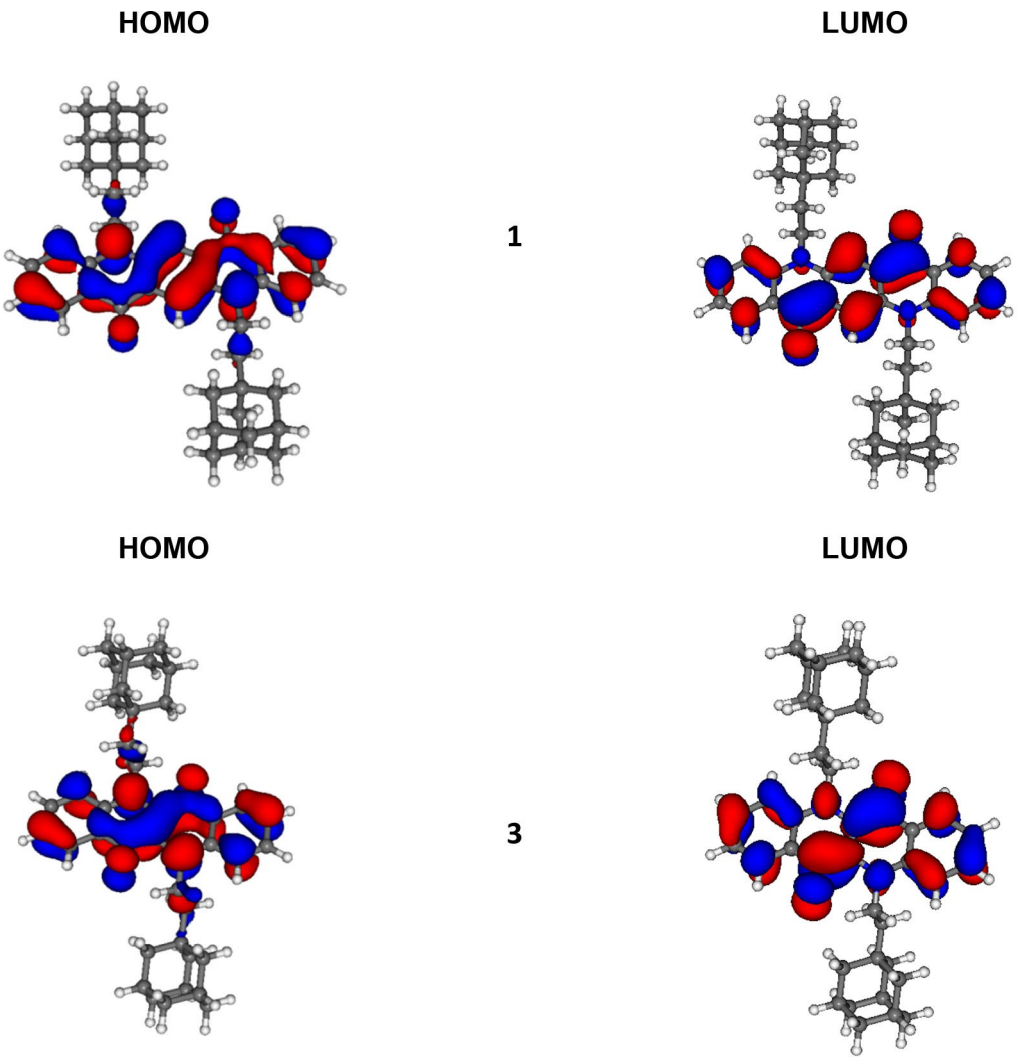

Figure 4. The shape of B3LYP frontier molecular orbitals of molecules **1** and **3** evaluated for the gas phase. The depicted iso-surface is 0.025 a.u.

values of electron-hole mobilities, i.e. from 0.15 to 1.27 $cm^2 V^{-1} s^{-1}$, are indicated for investigated dimers. It seems that the planarity deformation of the epindolidione core can support electron transport between the parallel-oriented subsystems.

2.4. Optical properties

Optical properties of novel dyes were also studied using UV-Vis and photoluminescence spectroscopy. Compared to the **QA** and **EPI**,[2] these molecules are not soluble in DMSO, thus optical measurements were performed in chloroform and toluene solutions. The recorded spectra are shown in Figure 5 (for chloroform) and Figure S7 (for toluene). In all cases, a vibronic structure is apparent from the spectra at the concentration of approximately 0.01 mM. The absorption maxima for compounds substituted by methyladamantyl are lower than 490 nm.[2] The wavelengths higher than 510 nm are connected with the presence of more flexible ethyladamantyl groups. For all four derivatives, a stronger absorption at lower wavelengths (ca. 300 nm) occurred relative to their absorption maxima at 480 and 560 nm. Interestingly, the wavelength reported in DMSO for **EPI** is 436 nm and for **QA** it is 527 nm.

The emission spectra were recorded at excitation wavelength 480 nm for **1** and **2**, while the excitation wavelength 560 nm was used for **3** and **4**. In general, the solvatochromic effect in optical properties was observed between the measurements in chloroform and toluene. When the material was dissolved in toluene, the spectra were blue-shifted compared to chloroform (Table 3). It is worth noting that no differences in excitation nor emission spectra were observed for different concentrations of solutions; the spectra are not presented. Furthermore, it is important to point out that UV-Vis spectra do correspond to the excitation spectra. An influence of different incorporation of side chains was observed. Adamantylethyl-substituted dyes **1** and **3** exhibited blue-shifted emission spectra compared to adamantylmethyl-substituted derivatives **2** and **4**. Interestingly, the bathochromic shift was more significant for epindolidione analogues **3** and **4** with the shift of

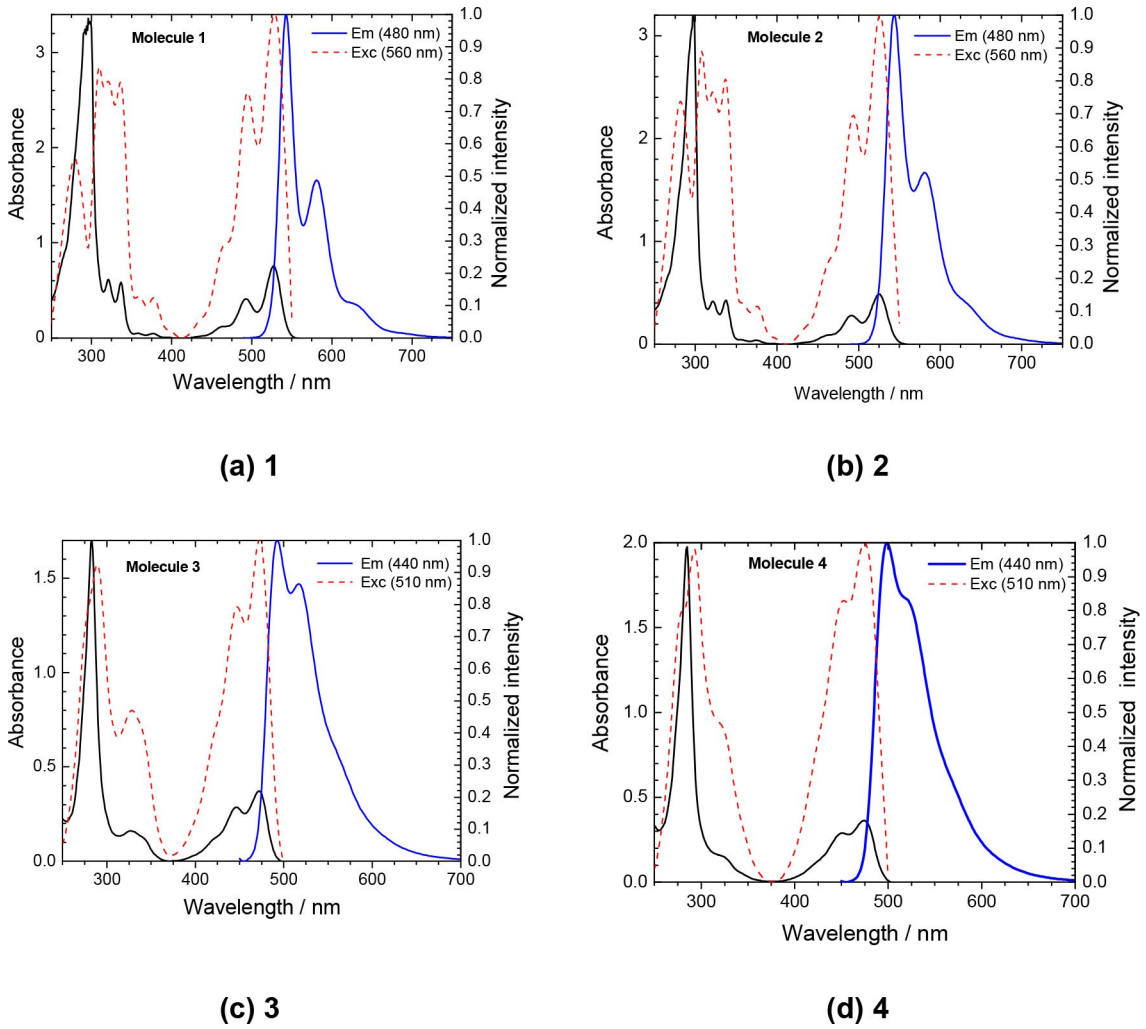

Figure 5. Absorption (black lines, left axis), excitation (blue lines, right axis) and emission (red lines, right axis) spectra of adamantyl-substituted dyes **1**–**4** in chloroform. The absorbance and normalized intensities are in arbitrary units.

Table 3. The theoretical TD–B3LYP absorption and fluorescence wavelength maxima (in nm) corresponding to the lowest energy transitions calculated for the gas phase, toluene and chloroform. The oscillator strengths are in parentheses.

	Absorption			Fluorescence		
	Gas	Toluene	Chloroform	Gas	Toluene	Chloroform
QA	447 (0.07)	463 (0.10)	470 (0.10)	478 (0.07)	498 (0.10)	514 (0.13)
EPI	399 (0.09)	408 (0.13)	411 (0.13)	428 (0.09)	441 (0.13)	452 (0.17)
1	461 (0.09)	475 (0.13)	481 (0.13)	491 (0.09)	509 (0.13)	524 (0.16)
2	459 (0.08)	472 (0.12)	479 (0.12)	493 (0.08)	509 (0.11)	524 (0.14)
3	425 (0.13)	433 (0.17)	435 (0.17)	465 (0.13)	477 (0.17)	488 (0.20)
4	431 (0.10)	440 (0.14)	442 (0.14)	480 (0.10)	490 (0.14)	500 (0.17)

6.9 and 9.6 nm for chloroform and toluene solution, respectively. On the contrary, for quinacridone-based derivatives **1** and **2**, the shift was only 1.3 and 0.5 nm for chloroform and toluene solution, respectively. The quantum chemical calculations of the optical transitions indicate that the vertical lowest energy transition ($S_0 \rightarrow S_1$) comes mainly from HOMO to LUMO electron excitation. As it is demonstrated in Table 3, the corresponding oscillator strengths have significant values. Similarly, the lowest energy de-excitation vertical transition ($S_1 \rightarrow S_0$) is well distinguished from the next electronic excited states and it has significant oscillator strength. When one compares with the reference **QA** and **EPI** molecules, the side substitution increases the maximal wavelengths of the absorption and fluorescence spectra. The solvatochromic shifts were also predicted from the calculations using the implicit solvent model.

Optical properties of the studied novel dyes were also studied in the solid phase, measured on uncrushed powder samples. Absorption spectra were also measured in thin films (Figure S8), but their quality was poor (see the Supporting

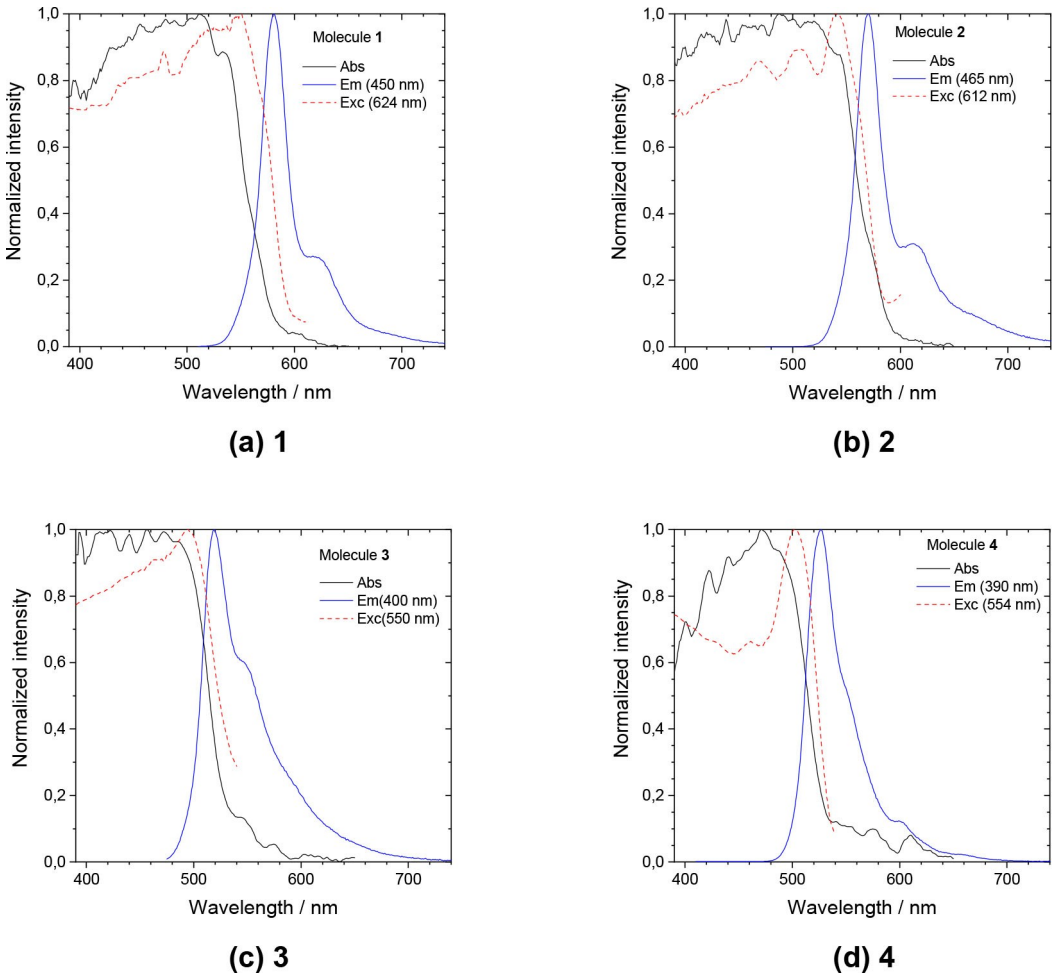

Figure 6. Solid-phase absorption spectra (Abs), excitation (Exc) and emission (Em) spectra of the studied compounds.

Information). In this experiment, the optical properties of the measured samples represent the superposition of molecular electronic structure and the averaged effect of aggregated molecules on the investigated sample surface. These measurements are more relevant for the possible application of molecules in optoelectronic devices or optical sensors. The recorded absorption spectra are bathochromically shifted with respect to those obtained in both solutions. The presented lowest energy bands are very broad and less structured. The recorded spectra were noisy due to the nature of the powder and the small amount of the measured samples. The spectra were digitally smoothed for better clarity. As shown in Figure 6, the determination of the corresponding absorption maximum position suffered from a large degree of uncertainty. Therefore, the more suitable characterization of these bands is connected with the determination of absorption edges (Table 4). The fluorescence spectra taken at different excitation energies show the bands with a vibronic structure that is comparable with solvated samples. The excitation wavelengths were chosen to accommodate for two effects. Firstly, the low Stokes shift of studied materials requires choosing a lower wavelength than the maximum of absorption to record the full emission spectrum, and secondly, wavelengths that are strong in the spectrum of the exciting lamp were chosen to obtain stronger emission. The investigated powder samples of *trans*-epindolidione derivatives exhibit efficient fluorescence. The absolute fluorescence quantum yield values range from 10% to 22% (see Table S1). The quantum yields of samples measured in chloroform range from 36% to 82% (see Table S2). It is worth highlighting the remarkable high PLQY values of 82% and 78% measured for alkylated quinacridones **1** and **2**, respectively.

Table 4. Wavelength maxima of optical spectra measured in solvated samples and powder samples. Global maxima and absorption edges (*) are set in bold and in italics, respectively. All values are written in nm.

Molecule	Environment	Absorption	Excitation	Emission
1	Chloroform	527, *545**	527	543
	Toluene	516, *530**	516	526
	Powder	*575**	550	581
2	Chloroform	527, *545**	527	545
	Toluene	514, *530**	516	526
	Powder	*580**	543	570
3	Chloroform	473, *489**	473	492
	Toluene	468, 482*	468	482
	Powder	*535**	494	519
4	Chloroform	475, *491**	474	499
	Toluene	470, *485**	468	492
	Powder	*533**	502	527

3. Conclusion

The one-step synthesis, quantum-chemical calculations, crystallographic, optical, electrochemical and thermal characterization of four novel air-stable adamantane-bearing dyes based on the epindolidione (**EPI**) and quinacridone (**QA**) cores were reported. Compared to the pristine **EPI** and **QA**, the simple one-step introduction of bulky methyladamantyl or ethyladamantyl groups blocks the formation of hydrogen bonds and fixes the planar dimer structures. On the other hand, the theoretical calculations predicted the stronger molecular packing ability in crystals of quinacridone derivatives due to the self-organizing effect of the highly symmetrical and rigid adamantane moiety via van der Waals interactions. For the epindolidione derivatives, the dimer interaction energies are lower due to the structural planarity perturbation of the central part. The observed high thermal stability can be explained due to the adamantyl-induced packing. The added substituents improve the solubility in comparison with its parent non-substituted molecules. The resulting electrochemical band gaps carried out on thin-film evaporated on ITO-coated glass electrodes were 2.4 to 2.5 eV. Compared to the reference **QA** and **EPI** molecules, the evaluated drift mobilities for the dimers selected from the X-ray structures indicate, according to the Marcus model, potentially better p-type and n-type electric intrinsic semiconduction. The experimental determination of real samples' semiconducting properties depends on many factors, e.g. sample processing or construction of probe transistors.[43] Therefore, systematic research into the electric mobilities of adamantyl derivatives **1**–**4** is planned in the future.

The prepared compounds exhibit remarkable fluorescence properties and efficiency in solution as well as in powder samples. The theoretical investigation quantified how the adamantyl substitution changes the chemical and electronic structure of benzothiadiazole-based cores.

The X-ray analyses show the existence of dimer-structures for molecules **1** and **2** with mutually coplanar oriented aromatic core centers. The quantum chemical simulations of these model dimers indicated possible *n*-type semiconductivity compared to unsubstituted parent molecules. On the other hand, the X-ray structure of **EPI** derivatives shows a strong interaction between adamantyl species, supporting the uniform separation of aromatic core centers. The spectroscopic measurements confirm better fluorescence properties than the **QA** derivatives. Based on the experimental observations and theoretical calculations, it is plausible to suggest molecule **1** for the investigation of electrical properties and molecule **3** as a building block for applied photonics research.

The hydrogen-bonded pigments such as Indigo, Epindolidione and Quinacridone are in their pristine form not soluble and not processable. In VAT dying processes they are normally processed by chemical reducing agents. The final color and pristine state is then established by the air-drying process with reoxidation using air oxygen. There is surely a great need for making such dyes solution-processable for printing, coating as well as for controlled crystallization. Such a side-chain substitution with adamantane side groups will make an impact on this general problem of solution processing of the pigment dyes.

Experimental Section

Materials and equipment

All solvents and reagents were obtained commercially and used as received unless stated otherwise. All moisture-sensitive reactions were performed in dry flasks fitted with glass stoppers or rubber septa under a positive pressure of argon. Solvents used for purification (petroleum ether, dichloromethane and methanol) were obtained from Penta Chemicals (Czech Republic) in p.a. grade. Flash column chromatography was performed using 220–440 mesh silica gel. Thin-layer chromatography was conducted on Supelco 60 TLC plates (Sigma Aldrich, St. Louis, MO, USA) with a 254 nm fluorescent indicator. Spots were observed under ultraviolet irradiation (254 nm or 354 nm). ^{1}H NMR spectra were recorded in $CDCl_3$ using an Avance III 300 MHz spectrometer (Bruker, Billerica, MA, USA) with working frequency of 300 MHz at 30 °C. Chemical shifts are expressed in parts per million (δ scale) downfield from tetramethylsilane and are referenced to residual protons in the NMR solvent ($CHCl_3$: δ = 7.25 ppm). Coupling constants (*J*) are given in Hz with coupling expressed as s-singlet, bs-broad singlet, d-doublet, dd-doublet of doublet, t-triplet, tdd-doublet of triplet of doublets, ddd-doublet of doublet of doublets, m-multiplet. Elemental analysis was performed using an EuroEA3000 Elemental Analyser (Eurovector, Pavia, Italy). Melting points were determined using a Kofler apparatus equipped with a Nagema PHMK 05 microscope (Nagema, Dresden, Germany), and the temperatures were not corrected. Thermogravimetric analysis was performed using TGA Q50 instrument (TA Instruments, New Castle, DE, USA) with nitrogen as the carrier gas.

Synthesis

General procedure for the N,N′-dialkylated dyes: A corresponding pigment (1.5 mmol, 1 equiv.) was mixed with cesium carbonate (6.0 mmol, 4 equiv.) in 15 mL of dry DMF under an argon atmosphere. The mixture was stirred at 110 °C for 2 h. Subsequently, 1-(2-bromoethyl)adamantane or 1-(bromomethyl) adamantane (6.0 mmol, 4 equiv.), respectively, was added and the reaction mixture was heated to 130 °C for 72 h. After cooling to room temperature, the reaction mixture was poured into water (250 mL) and sonicated for 30 min. The suspension was filtered, providing a solid crude product that was dried at room temperature under a high vacuum. The crude product was adsorbed on silica gel and purified by column chromatography, followed by purification by boiling in methanol and filtration of as-obtained solid in the formed suspension to yield the corresponding *N,N′*-dialkylated dye. The measured ^{1}H and ^{13}C NMR spectra of the resulting products (**1**–**4**) are depicted in the *Supporting information* as Figures S9–S14.

5-(2-((1r,3R,5S)-adamantan-1-yl)ethyl)-12-(2-((3r,5r,7r)-adamantan-1-yl)ethyl)-5,12-dihydroquinolino[2,3-b]acridine-7,14-dione (1): Compound **1** was synthesized according to the General Procedure. The reaction of quinacridone (1.50 g, 4.80 mmol) with cesium carbonate (10.43 g, 19.2 mmol) and 1-(2-bromoethyl)adamantane (4.67 g, 19.2 mmol) provided crude compound **1**. The crude product was purified by silica gel chromatography using gradient elution by a mixture of petroleum ether/dichloromethane (20/80→10/90→0/100). The component with R_f = 0.5 (DCM) was subsequently boiled in methanol (50 mL), cooled, and filtered to yield compound **1** as a bright orange solid (yield 1.75 g, 57 %). Melting

point > 330 °C. ^{1}H NMR (500 MHz, $CDCl_3$, TMS): δ = 8.80 (s, 2H), 8.59 (dd, *J* = 8.1, 1.8 Hz, 2H), 7.77 (ddd, *J* = 8.8, 6.9, 1.8 Hz, 2H), 7.53 (d, *J* = 8.8 Hz, 2H), 7.28 (t, *J* = 7.4 Hz, 2H), 4.60 (t, *J* = 8.9 Hz, 4H), 2.15–2.10 (m, 6H), 1.87 (d, *J* = 2.8 Hz, 12H), 1.79 (d, *J* = 3.9 Hz, 6H), 1.55 (s, 10H). ^{13}C NMR (126 MHz, $CDCl_3$): δ = 178.39, 142.46, 135.82, 134.82, 128.31, 126.70, 121.44, 120.95, 114.50, 113.56, 42.41, 41.81, 40.20, 37.22, 32.63, 28.78. Elemental analysis calc. (%) for $C_{44}H_{48}N_2O_2$: C 82.98, H 7.60, N 4.40; found: C 82.96, H 7.61, N 4.41.

5,12-bis(adamantan-1-ylmethyl)-5,12-dihydroquinolino[2,3-b]-acridine-7,14-dione (2): Compound **2** was synthesized according to the General Procedure. The reaction of quinacridone (0.75 g, 2.40 mmol) with cesium carbonate (5.22 g, 9.61 mmol) and 1-(bromomethyl)adamantane (2.20 g, 9.61 mmol) provided crude compound **2**. The crude product was purified by silica gel chromatography using dichloromethane as the eluent. The component with R_f = 0.5 (DCM) was subsequently boiled in methanol (50 mL), cooled and filtered to yield compound **2** as a bright orange solid (yield 0.38 g, 25 %). Melting point > 330 °C. ^{1}H NMR ($CDCl_3$, TMS): δ = 9.04 (s, 2H), 8.60 (dd, J = 7.7, 2.2 Hz, 2H), 7.78 (d, J = 8.8 Hz, 2H), 7.74–7.70 (m, 2H), 7.35–7.26 (m, 2H), 4.67–4.60 (m, 2H), 4.39 (dd, J = 16.3, 8.8 Hz, 2H), 1.95–1.89 (m, 2H), 1.73–1.50 (m, 28H). Elemental analysis calc. (%) for $C_{42}H_{44}N_2O_2$: C 82.86, H 7.28, N 4.60; found: C 82.84, H 7.25, N 4.64.

5-(2-((1r,3R,5S)-adamantan-1-yl)ethyl)-11-(2-((3r,5r,7r)-adamantan-1-yl)ethyl)-5,11-dihydrodibenzo[b,g][1,5]naphthyridine-6,12-dione (3): Compound **3** was synthesized according to the General Procedure. The reaction of epindolidione (0.70 g, 2.67 mmol) with cesium carbonate (5.80 g, 10.7 mmol) and 1-(2-bromoethyl) adamantane (2.60 g, 10.7 mmol) provided crude compound **3**. The crude product was purified by silica gel chromatography using gradient elution by a mixture of petroleum ether/dichloromethane (50/50→40/60). The component with R_f = 0.4 (PE/DCM 50/50) was subsequently boiled in methanol (30 mL), cooled and filtered to yield compound **3** as a bright green-yellow solid (yield 0.42 g, 29 %). Melting point > 330 °C. ^{1}H NMR ($CDCl_3$, TMS): δ = 8.44 (d, J = 8.1 Hz, 2H), 7.72–7.71 (m, 4H), 7.35–7.28 (m, 2H), 5.00–4.97 (m, 4H), 1.99 (s, 6H), 1.75–1.64 (m, 24H), 1.60–1.57 (m, 4H). ^{13}C NMR (126 MHz, $CDCl_3$): δ = 175.01, 141.93, 133.39, 132.34, 127.51, 126.15, 122.14, 116.38, 44.77, 43.10, 42.46, 37.26, 32.52, 28.79. Elemental analysis calc. (%) for $C_{40}H_{46}N_2O_2$: C 81.87, H 7.90, N 4.77; found: C 81.85, H 7.87, N 4.81.

5,11-bis(adamantan-1-ylmethyl)-5,11-dihydrodibenzo [b,g][1,5]naphthyridine-6,12-dione (4): Compound **4** was synthesized according to the General Procedure. The reaction of epindolidione (1.00 g, 3.81 mmol) with cesium carbonate (8.28 g, 15.3 mmol) and 1-(bromomethyl)adamantane (3.50 g, 15.3 mmol) provided crude compound **4**. The crude product was purified by three-step silica gel chromatography using elution mixture PE/DCM (25/75; 10/90; 10/90). The component with R_f = 0.4 (PE/DCM 25/75) was subsequently boiled in methanol (15 mL), cooled and filtered to yield compound **3** as a bright green-yellow solid (yield 0.26 g, 17 %). Melting point > 330 °C. ^{1}H NMR ($CDCl_3$, TMS): δ = 8.32 (d, J = 8.1 Hz, 2H), 7.84 (d, J = 8.8 Hz, 2H), 7.65 (ddd, J = 8.7, 6.8, 1.7 Hz, 2H), 7.31 (d, J = 7.4 Hz, 2H), 5.78 (d, J = 15.4 Hz, 2H), 4.26 (d, J = 15.4 Hz, 2H), 1.66 (br s, 6H), 1.49–1.31 (m, 12H), 1.20–1.04 (m, 12H). Elemental analysis calc. (%) for $C_{38}H_{42}N_2O_2$: C 81.68, H 7.58, N 5.01; found: C 81.64, H 7.55, N 4.98.

X-ray diffraction

The crystals suitable for X-ray analysis were prepared by controlled crystallization from the saturated solutions of the alkylated dyes **1** to **4** in chlorobenzene. The XRD data were collected at temperature 120 K by the ω-scan technique on a Rigaku Saturn724 + CCD diffractometer equipped with an Oxford Cryosystem low-temperature device, using a rotating anode with MoKα radiation. The diffraction intensities were corrected for Lorentz and polarization effects, and an analytical method of absorption was used. Data interpretation, including all corrections mentioned previously, was performed by CrystalClear-SM Expert 2.1 b32 software (Rigaku, 2014). The structures were resolved in a straightforward manner by direct methods and refined by the full-matrix least-squares method on all F2 data. Non-hydrogen atoms were refined anisotropically, while hydrogen atoms were inserted in the calculated positions and refined isotropically, assuming a "ride-on" model. The SHELXS and SHELXL programs used for calculations and the XP program used for geometrical analysis were parts of the Bruker SHELXTL V5.1 program package.

Deposition numbers 2035461, 2035462, 2035463, and 2035464 contain the supplementary crystallographic data for this paper. These data are provided free of charge by the joint Cambridge Crystallographic Data Centre and Fachinformationszentrum Karlsruhe Access Structures service.[44]

Quantum chemical calculations

The quantum chemical calculations were performed using Gaussian 16 program package.[45] The optimal geometries were calculated by DFT method with hybrid B3LYP (Becke's three parameter Lee-Yang-Parr) functional[46,47] without any constraints (energy cut-off of 10^{-5} kJ mol^{-1}, final RMS energy gradient under 0.01 kJ mol^{-1} A^{-1}). The 6-31G(d,p) basis set of atomic orbitals was applied for all atoms.[48] If available, X-ray structures were taken as the input geometries of studied molecules and were symmetrized. The corresponding point group symmetry was used as the starting symmetry of geometry for the optimization procedure (see Figure 1). The optimized structures were confirmed to be stable by vibrational analysis (no imaginary frequencies). Based on optimized B3LYP geometries, the vertical transition energies and oscillator strengths between the initial and final electronic states were computed using the time-dependent (TD)-DFT method.[49] The TD-DFT approach was also used to calculate the electronic lowest-excited geometries and corresponding de-excitation energies. The ultrafine setting for the integration grid was used for all calculations. Solvent effects in chloroform and toluene were approximated by Solvation Model based on Density (SMD).[50] The interaction energies for molecular dimers selected from X-ray structures were corrected for the Basis Set Superposition Error (BSSE)[51] using the Counterpoise method .[52] For the used DFT functional, we have used the Grimme's dispersion correction with Becke-Johnson damping function (GD3BJ).[53] For selected X-ray dimers, the charge transport properties were evaluated using the hopping model[54–56] based on the Marcus formula[57] (see the Supporting information). The optimal geometries of electroneutral molecules and molecular orbitals were visualized using the Molekel program package.[58]

Electrochemical measurements

The Highest Occupied Molecular Orbital (HOMO) and Lowest Unoccupied Molecular Orbital (LUMO) energy levels of all compounds were determined electrochemically using cyclic voltammetry. The experiments were performed in three-electrode electrochemical using a Jaissle Potentiostat-Galvanostat IMP 83 (Jaissle Elektronik GmbH, Waiblingen, Germany). The setup consisted of an indium tin oxide-coated glass slide deposited with the respective compound as a working electrode, a Ag/AgCl quasi-reference electrode (QRE) and a Pt plate counter electrode. As an electrolyte solution 0.1 M tetrabutylammoniumhexafluorophosphate ($TBAPF_6$)

in anhydrous acetonitrile was used. Cyclic voltammograms were recorded at scanning potential from 0 to 2.0 V vs Ag/AgCl QRE for the determination of HOMO energy level (E_{HOMO}) and from 0 to −2.0 V vs Ag/AgCl QRE for the determination of LUMO energy level (E_{LUMO}) with the scanning rate of 25 mVs^{-1}. The potentials were calibrated externally against ferrocene/ferrocenium redox couple of 0.69 V vs normal hydrogen electrode (NHE) in acetonitrile solution .[59] The energy levels were calculated using the following formula for onset potentials [Eqs. (1) and (2)].[60]

$$E_{HOMO} = -\left(4.75eV + E_{ox,onset}vsNHE\right) \quad (1)$$

$$E_{LUMO} = -\left(4.75eV + E_{,onset}vsNHE\right) \quad (2)$$

Optical measurements

Ultraviolet-Visible (UV-Vis) and fluorescence spectroscopy were used to determine the optical properties of the alkylated quinacridone and epindolidione dyes. To measure the spectra of the solutions, including evaluation of the molar absorption coefficient of each material, a set of solutions in chloroform or toluene (optical quality) were prepared with the concentrations of 0.050 and 0.003 mM in chloroform, or 0.030 and 0.002 mM in toluene, respectively. The used solvents, chloroform and toluene (spectroscopic purity) were purchased from Sigma-Aldrich, Germany. The UV-Vis absorption spectroscopy was performed with Lambda1050 UV/Vis/NIR spectrometer (PerkinElmer). Fluorescence spectra were obtained with a fluorimeter QuantaMaster 40 from Photon Technology International. Measurements were performed using quartz cuvettes with a path length of 10.00 mm.

Absorption measurements of powder samples were carried out using a U-3900H (Hitachi) UV-Vis spectrophotometer with an attached Integration sphere module. The absorption spectra were determined from diffuse reflectance measurement automatically by the measurement software. The samples were sandwiched between glass slides and loaded into the integrating sphere. The light was incident at an angle of 0°. The reflected light was collected by integrating the sphere.

Photoluminescence measurements were carried out using a Fluorolog (Horiba JY) fluorimeter. The powder samples were put into a sample holder and covered with a covering glass to be held in place. The excitation light was incident at an angle of 30°, while the luminescence was collected at 90° relative to the excitation. Quantum yields of photoluminescence (PLQY) were determined by an absolute method using a Quanta-Phi integrating sphere and Fluorolog fluorimeter (both Horiba JY). The absolute method does not require PLQY standard, as quantum yields are obtained by detecting all sample fluorescence through the use of an integrating sphere. For PLQY measurements the samples were put on a glass and loaded into the integrating sphere. The excitation light was incident at an angle of 0°; the luminescence was collected by the integrating sphere. It should be noted that the sensitivity of the integrating sphere is not high, giving rise to a high absolute error; this is particularly problematic in low PLQY samples. The optical measurements were done under ambient conditions.

Acknowledgments

The authors thank for their financial support the Ministry of Industry and Trade TRIO (project No. FV20022), the Austrian Agency for International Cooperation in Education and Research (OEAD-GmbH, WTZ, CZ01/2020, 8J20AT025), the Slovak Research and Development Agency (APVV-19-0024) and the Slovak Grant Agency (VEGA 1/0461/21). V.L. thanks the Ministry of Education, Science, Research and Sport of Slovakia for funding under the Excellent Research Teams schema. J.R., J.K. and M.W. thank project 21-01057S from Czech Science Foundation. CIISB, Instruct-CZ Centre of Instruct-ERIC EU consortium, funded by MEYS CR infrastructure project LM2018127, is gratefully acknowledged for financial support for the single crystal diffraction measurements at the X-ray Diffraction and Bio-SAXS Core Facility of CEITEC Masaryk University. The authors thank Dr. Jan Rohlíček from the Institute of Physics CAS Prague for X-ray measurements. Financial support of the Austrian Science Foundation (FWF) within the Wittgenstein Prize (Z222-N19) for Prof. Sariciftci is gratefully acknowledged.

Conflict of Interest

The authors declare no conflict of interest.

Keywords: Molecular designing · Adamantyl induced packing · Organic pigments · UV-Vis spectroscopy · Fluorescence

[1] P. Harrop, J. Hayward, R. Das, G. Holland, Wearable Technology 2015–2025: Technologies, Markets, Forecasts. *IDTechEx report* **2015**.
[2] E. D. Glowacki, M. Irimia-Vladu, S. Bauer, N. S. Sariciftci, *J. Mater. Chem. B* **2013**, *1*, 3742–3753.
[3] M. Irimia-Vladu, E. D. Glowacki, N. S. Sariciftci, S. Bauer, ed. *Green materials for electronics*. Weinheim: Wiley-VCH, **2018**. ISBN 978–3-527-33865–8.
[4] A. Tang, Ch. Zhan, J. Yao, E. Zhou, *Adv. Mater.* **2017**, *29*, 1600013.
[5] Z. Yi, S. Wang, Y. Liu, *Adv. Mater.* **2015**, *27*, 3589–3606.
[6] Ch. B. Nielsen, M. Turbiez, I. McCulloch, *Adv. Mater.* **2013**, *25*, 1859–1880.
[7] N. M. Randell, T. L. Kelly, *Chem. Rec.* **2019**, *19*, 973–988.
[8] W. Herbst, K. Hunger, *Industrial Organic Pigments: Production, Properties, Applications.* 3rd Ed ., Wiley-VCH, Weinheim, Germany **2006**. ISBN: 978–3-527-60406-7.
[9] M. Gsänger, D. Bialas, L. Huang, M. Stolte, F. Würthner, *Adv. Mater.* **2016**, *28*, 3615–3645.
[10] C. Wang, Z. Zhang, Y. Wang, *J. Mater. Chem. C* **2016**, *4*, 9918–9938.
[11] D. Lüftner, S. Refaely-Abramson, M. Pachler, R. Resel, M. G. Ramsey, L. Kronik, P. Puschnig, *Phys. Rev. B* **2014**, *90*, 075204.
[12] H. J. Song, D. H. Kim, E. J. Lee, S. W. Heo, J. Y. Lee, D. K. Moon, *Macromolecules* **2012**, *45*, 7815–7822.
[13] E. D. Głowacki, L. Leonat, M. Irimia-Vladu, R. Schwödiauer, M. Ullah, H. Sitter, S. Bauer, N. S. Sariciftci, *Appl. Phys. Lett.* **2012**, *101*, 023305.
[14] E. D. Głowacki, M. Irimia-Vladu, M. Kaltenbrunner, J. Gasiorowski, M. S. White, U. Monkowius, G. Romanazzi, G. P. Suranna, P. Mastrorilli, T. Sekitani, S. Bauer, T. Someya, L. Torsi, N. S. Sariciftci, *Adv. Mater.* **2013**, *25*, 1563–1569.
[15] A. O. F. Jones, Ch. Röthel, R. Lassnig, O. N. Bedoya-Martinez, P. Christian, I. Salzmann, B. Kunert, A. Winkler, R. Resel, *CrystEngComm* **2017**, *19*, 1902–1911.
[16] R. Lassnig, B. Striedinger, A. O. F. Jones, B. Scherwitzl, A. Fian, E. D. Głowacki, B. Stadlober, A. Winkler, *Synth. Met.* **2016**, *218*, 64–74.
[17] D. S. Weiss, M. Burberry, *Thin Solid Films* **1988**, *158*, 175–187.
[18] D. S. Filho, C. M. F. Oliveira, *J. Mater. Sci.* **1992**, *27*, 5101–5107.
[19] T. Wagner, M. Györök, D. Huber, P. Zeppenfeld, E. D. Głowacki, *J. Phys. Chem. C* **2014**, *118*, 10911–10920.
[20] Y. Cui, G. Liang, J. Jia, G. Yu, Y. Sha, Ch. Zhou, Y. She, *Tetrahedron* **2020**, *76*, 131169.
[21] B. Scherwitzl, Ch. Röthel, A. O. F. Jones, B. Kunert, I. Salzmann, R. Resel, G. Leising, A. Winkler, *J. Phys. Chem. C* **2015**, *119*, 20900–20910.

[22] M. Koehler, D. Farka, C. Yumusak, N. S. Sariciftci, P. Hinterdorfer, *ChemPhysChem* **2020**, *21*, 659–666.
[23] S. E. Shaheen, B. Kippelen, N. Peyghambarian, *J. Appl. Phys.* **1999**, *85*. 7939–7945.
[24] E. del Puerto, C. Domingo, S. Sanchez-Cortes, J. V. García-Ramos, R. F. Aroca, *J. Phys. Chem. C* **2011**, *115*, 16838–16843.
[25] P. Zalar, T. V. Pho, A. Garcia, B. Walker, W. Walker, F. Wudl, T.-Q. Nguyen, *J. Phys. Chem. C* **2011**, *115*, 17533–17539.
[26] K.-H. Lee, G. H. Lee, D.-S. Leem, J. Lee, J. W. Chung, X. Bulliard, H. Choi, K.-B. Park, K.-S. Kim, Y. W. Jin, S. Lee, S. Y. Park, *J. Phys. Chem. C* **2014**, *118*, 13424–13431.
[27] Y. Liu, L. Wang, J. Zhou, S. Wu, Y. Wei, A. Chang, X. Liu, *Dyes Pigm.* **2015**, *121*, 328–335.
[28] S. Stříteský, M. Vala, J. David, E. Šafaříková, J. Víteček, M. Weiter, *Chem. Pap.* **2018**, *72*, 1635–1643.
[29] K. Ye, J. Wang, H. Sun, Y. Liu, Z. Mu, F. Li, S. Jiang, J. Zhang, H. Zhang, Y. Wang, C.-M. Che, *J. Phys. Chem. B* **2005**, *109*, 8008–8016.
[30] M. Sytnyk, E. D. Głowacki, S. Yakunin, G. Voss, W. Schöfberger, D. Kriegner, J. Stangl, R. Trotta, C. Gollner, S. Tollabimazraehno, G. Romanazzi, Z. Bozkurt, M. Havlicek, N. S. Sariciftci, W. Heiss, *J. Am. Chem. Soc.* **2014**, *136*, 16522–16532.
[31] E. Miglbauer, N. Demitri, M. Himmelsbach, U. Monkowius, N. S. Sariciftci, E. D. Głowacki, K. T. Oppelt, *ChemistrySelect* **2016**, *1*, 6349–6355.
[32] J. David, M. Weiter, M. Vala, J. Vyňuchal, J. Kučerík, *Dyes Pigm.* **2011**, *89 (2)*, 137–143.
[33] Y. Hong, J. W. Y. Lam, B. Z. Tang, *Chem. Soc. Rev.* **2011**, *40*, 5361–5388.
[34] J. Mei, N. L. C. Leung, R. T. K. Kwok, J. W. Y. Lam, B. Z. Tang, *Chem. Rev.* **2015**, *115*, 11718–11940.
[35] C. Wang, K. Wang, Q. Fu, J. Zhang, D. Ma, Y. Wang, *J. Mater. Chem. C* **2013**, *1*, 410–413.
[36] Z.-X. Xu, H.-F. Xiang, V. A. L. Roy, S. S.-Y. Chui, Y. Wang, P. T. Lai, Ch.-M. Che, *Appl. Phys. Lett.* **2009**, *95*, 123305.
[37] T. Marszalek, I. Krygier, A. Pron, Z. Wrobel, P. M. W. Blom, I. Kulszewicz-Bajer, W. Pisula, *Org. Electron.* **2019**, *65*, 127–134.
[38] J. Krajčovič, A. Kovalenko, P. Heinrichová, M. Vala, M. Weiter, *J. Lumin.* **2016**, *175*, 94–99.
[39] A. Kovalenko, C. Yumusak, P. Heinrichová, S. Stříteský, L. Fekete, M. Vala, M. Weiter, N. S. Sariciftci, J. Krajčovič, *J. Mater. Chem. C* **2017**, *5*, 4716–4723.
[40] D. R. Cooper, B. D'Anjou, N. Ghattamaneni, B. Harack, M. Hilke, A. Horth, N. Majlis, M. Massicotte, L. Vandsburger, E. Whiteway, V. Yu, *Condens. Matter Phys.* **2012**, 1–56.
[41] E. D. Głowacki, G. Romanazzi, C. Yumusak, H. Coskun, U. Monkowius, G. Voss, M. Burian, R. T. Lechner, N. Demitri, G. J. Redhammer, N. Sünger, G. P. Suranna, N. S. Sariciftci, *Adv. Funct. Mater.* **2015**, *25*, 776–787.
[42] V. Lukeš, D. Cagardová, M. Michalík, P. Poliak, *Synth. Met.* **2018**, *240*, 67–76.
[43] M. Irimia-Vladu, Y. Kanbur, F. Camaioni, M. E. Copolla, C. Yumusak, C. V. Irimia, A. Vlad, A. Operamolla, G. M. Farinola, G. P. Suranna, N. González-Benitez, M. C. Molina, L. F. Bautista, H. Langhals, B. Stadlober, E. D. Głowacki, N. S. Sariciftci, *Chem. Mater.* **2019**, *31*, 6315–6346.
[44] Copies of the data can be obtained, free of charge, on application to the Director, CCDC, 12 Union Road, Cambridge CB2 1EZ, UK (fax: +44-(0)1223-336033 or e-mail: deposit@ccdc.cam.ac.uk).
[45] Gaussian 16, Revision A.03, M. J. Frisch, G. W. Trucks, H. B. Schlegel, G. E. Scuseria, M. A. Robb, J. R. Cheeseman, G. Scalmani, V. Barone, G. A. Petersson, H. Nakatsuji, X. Li, M. Caricato, A. V. Marenich, J. Bloino, B. G. Janesko, R. Gomperts, B. Mennucci, H. P. Hratchian, J. V. Ortiz, A. F. Izmaylov, J. L. Sonnenberg, D. Williams-Young, F. Ding, F. Lipparini, F. Egidi, J. Goings, B. Peng, A. Petrone, T. Henderson, D. Ranasinghe, V. G. Zakrzewski, J. Gao, N. Rega, G. Zheng, W. Liang, M. Hada, M. Ehara, K. Toyota, R. Fukuda, J. Hasegawa, M. Ishida, T. Nakajima, Y. Honda, O. Kitao, H. Nakai, T. Vreven, K. Throssell, J. A. Montgomery, Jr., J. E. Peralta, F. Ogliaro, M. J. Bearpark, J. J. Heyd, E. N. Brothers, K. N. Kudin, V. N. Staroverov, T. A. Keith, R. Kobayashi, J. Normand, K. Raghavachari, A. P. Rendell, J. C. Burant, S. S. Iyengar, J. Tomasi, M. Cossi, J. M. Millam, M. Klene, C. Adamo, R. Cammi, J. W. Ochterski, R. L. Martin, K. Morokuma, O. Farkas, J. B. Foresman, D. J. Fox, Gaussian, Inc., Wallingford CT, **2016**.
[46] Ch. Lee, W. Yang, R. G. Parr, *Phys. Rev. B* **1988**, *37*, 785–789.
[47] A. D. Becke, *Phys. Rev. A* **1998**, *38*, 3098–3100.
[48] P. C. Hariharan, J. A. Pople, *Theor. Chim. Acta.* **1973**, *28*, 213–222.
[49] F. Furche, R. Ahlrichs, *J. Chem. Phys.* **2002**, *117*, 7433–7447.
[50] A. V. Marenich, Ch. J. Cramer, D. G. Truhlar, *J. Phys. Chem. B* **2009**, *113*, 6378–6396.
[51] S. F. Boys, F. Bernardi, *Mol. Phys.* **2006**, *19*, 553–566.
[52] S. S. Xantheas, *J. Chem. Phys.* **1996**, *104*, 8821–8824.
[53] S. Grimme, S. Ehrlich, L. Goerigk, *J. Comb. Chem.* **2011**, *32*, 1456–1465.
[54] M. Malagoli, J.-L. Brédas, *Chem. Phys. Lett.* **2000**, *327*, 13–17.
[55] J.-L. Brédas, D. Beljonne, V. Coropceanu, J. Cornil, *Chem. Rev.* **2004**, *104*, 4971–5004.
[56] S. A. Maier, J. Ankerhold, *Phys. Rev. E* **2010**, *81*, 021107-1-14.
[57] R. A. Marcus, *Rev. Mod. Phys.* **1993**, *65*, 599–610.
[58] P. Flukiger, H. P. Luthi, S. Sortmann, J. Weber, Molekel 5.4.0.8. **2009**, *Swiss National Supercomputing Centre*, Manno, Switzerland.
[59] T. J. Smith, K. J. Stevenson, Reference Electrodes, in *Handbook of Electrochemistry* (Ed.: C. G. Zoski), Elsevier: Amsterdam, **2007**; 73–110.
[60] C. M. Cardona, W. Li, A. E. Kaifer, D. Stockdale, G. C. Bazan, *Adv. Mater.* **2011**, *23*, 2367–2371.

Manuscript received: June 10, 2021
Revised manuscript received: September 1, 2021
Accepted manuscript online: September 14, 2021
Version of record online: September 24, 2021